Measurement of the ^{72}Ge(n, γ) cross section over a wide neutron energy range at the CERN n_TOF facility

M. Dietz [1,*] C. Lederer-Woods,[1] A. Tattersall,[1] U. Battino,[1] F. Gunsing,[2,3] S. Heinitz,[4] M. Krtička,[5] J. Lerendegui-Marco,[6]
R. Reifarth,[7] S. Valenta,[5] O. Aberle,[3] S. Amaducci,[8,9] J. Andrzejewski,[10] L. Audouin,[11] M. Bacak,[12,3,2] J. Balibrea,[13]
M. Barbagallo,[14] F. Bečvář,[5] E. Berthoumieux,[2] J. Billowes,[15] D. Bosnar,[16] A. Brown,[17] M. Caamaño,[18] F. Calviño,[19]
M. Calviani,[3] D. Cano-Ott,[13] R. Cardella,[3] A. Casanovas,[19] F. Cerutti,[3] Y. H. Chen,[11] E. Chiaveri,[3,15,6] N. Colonna,[14]
G. Cortés,[19] M. A. Cortés-Giraldo,[6] L. Cosentino,[20] L. A. Damone,[14,21] M. Diakaki,[2] C. Domingo-Pardo,[22] R. Dressler,[4]
E. Dupont,[2] I. Durán,[18] B. Fernández-Domínguez,[18] A. Ferrari,[3] P. Ferreira,[23] P. Finocchiaro,[20] V. Furman,[24] K. Göbel,[7]
A. R. García,[13] A. Gawlik,[10] S. Gilardoni,[3] T. Glodariu,[25,†] I. F. Gonçalves,[23] E. González-Romero,[13] E. Griesmayer,[12]
C. Guerrero,[6] H. Harada,[26] J. Heyse,[27] D. G. Jenkins,[17] E. Jericha,[12] F. Käppeler,[28] Y. Kadi,[3] D. Kahl,[1] A. Kalamara,[29]
P. Kavrigin,[12] A. Kimura,[26] N. Kivel,[4] M. Kokkoris,[29] D. Kurtulgil,[7] E. Leal-Cidoncha,[18] H. Leeb,[12] S. Lo Meo,[30,8]
S. J. Lonsdale,[1] D. Macina,[3] A. Manna,[8,9] J. Marganiec,[10,31] T. Martínez,[13] A. Masi,[3] C. Massimi,[8,9] P. Mastinu,[32]
M. Mastromarco,[14] E. A. Maugeri,[4] E. Mazzone,[14,33] E. Mendoza,[13] A. Mengoni,[30] P. M. Milazzo,[34] F. Mingrone,[3]
A. Musumarra,[20,35] A. Negret,[25] R. Nolte,[31] A. Oprea,[25] N. Patronis,[36] A. Pavlik,[37] J. Perkowski,[10] I. Porras,[38] J. Praena,[38]
J. M. Quesada,[6] D. Radeck,[31] T. Rauscher,[39,40] C. Rubbia,[3] J. A. Ryan,[15] M. Sabaté-Gilarte,[3,6] A. Saxena,[41] P. Schillebeeckx,[27]
D. Schumann,[4] P. Sedyshev,[24] A. G. Smith,[15] N. V. Sosnin,[15] A. Stamatopoulos,[29] G. Tagliente,[14] J. L. Tain,[22]
A. Tarifeño-Saldivia,[19] L. Tassan-Got,[11] G. Vannini,[8,9] V. Variale,[14] P. Vaz,[23] A. Ventura,[8] V. Vlachoudis,[3] R. Vlastou,[29]
A. Wallner,[42] S. Warren,[15] C. Weiss,[12] P. J. Woods,[1] T. Wright,[15] and P. Žugec[16,3]

(n_TOF Collaboration)[‡]

[1]*School of Physics and Astronomy, University of Edinburgh, Edinburgh, United Kingdom*
[2]*CEA Irfu, Université Paris-Saclay, F-91191 Gif-sur-Yvette, France*
[3]*European Organization for Nuclear Research (CERN), Geneva, Switzerland*
[4]*Paul Scherrer Institut (PSI), Villingen, Switzerland*
[5]*Charles University, Prague, Czech Republic*
[6]*Universidad de Sevilla, Sevilla, Spain*
[7]*Goethe University Frankfurt, Frankfurt am Main, Germany*
[8]*Istituto Nazionale di Fisica Nucleare, Sezione di Bologna, Bologna, Italy*
[9]*Dipartimento di Fisica e Astronomia, Università di Bologna, Bologna, Italy*
[10]*University of Lodz, Lodz, Poland*
[11]*Institut de Physique Nucléaire, CNRS-IN2P3, Université Paris-Sud, Université Paris-Saclay, F-91406 Orsay Cedex, France*
[12]*Technische Universität Wien, Vienna, Austria*
[13]*Centro de Investigaciones Energéticas Medioambientales y Tecnológicas (CIEMAT), Madrid, Spain*
[14]*Istituto Nazionale di Fisica Nucleare, Sezione di Bari, Bari, Italy*
[15]*University of Manchester, Manchester, United Kingdom*
[16]*Department of Physics, Faculty of Science, University of Zagreb, Zagreb, Croatia*
[17]*University of York, York, United Kingdom*
[18]*University of Santiago de Compostela, Santiago de Compostela, Spain*
[19]*Universitat Politècnica de Catalunya, Barcelona, Spain*
[20]*INFN Laboratori Nazionali del Sud, Catania, Italy*
[21]*Dipartimento di Fisica, Università degli Studi di Bari, Bari, Italy*
[22]*Instituto de Física Corpuscular, CSIC - Universidad de Valencia, Valencia, Spain*
[23]*Instituto Superior Técnico, Lisbon, Portugal*
[24]*Joint Institute for Nuclear Research (JINR), Dubna, Russia*
[25]*Horia Hulubei National Institute of Physics and Nuclear Engineering, Bucharest, Romania*
[26]*Japan Atomic Energy Agency (JAEA), Tokai-mura, Japan*
[27]*European Commission, Joint Research Centre, Geel, Retieseweg 111, B-2440 Geel, Belgium*
[28]*Karlsruhe Institute of Technology, Campus North, IKP, 76021 Karlsruhe, Germany*

*Presently at Physikalisch-Technische Bundesanstalt (PTB), Bundesallee 100, 38116 Braunschweig, Germany; mirco.dietz@ptb.de
†Deceased.
‡www.cern.ch/ntof

^{29}*National Technical University of Athens, Athens, Greece*
^{30}*Agenzia Nazionale per le Nuove Tecnologie (ENEA), Bologna, Italy*
^{31}*Physikalisch-Technische Bundesanstalt (PTB), Bundesallee 100, 38116 Braunschweig, Germany*
^{32}*Istituto Nazionale di Fisica Nucleare, Sezione di Legnaro, Legnaro, Italy*
^{33}*Consiglio Nazionale delle Ricerche, Bari, Italy*
^{34}*Istituto Nazionale di Fisica Nucleare, Sezione di Trieste, Trieste, Italy*
^{35}*Dipartimento di Fisica e Astronomia, Università di Catania, Catania, Italy*
^{36}*University of Ioannina, Ioannina, Greece*
^{37}*University of Vienna, Faculty of Physics, Vienna, Austria*
^{38}*University of Granada, Granada, Spain*
^{39}*Department of Physics, University of Basel, Basel, Switzerland*
^{40}*Centre for Astrophysics Research, University of Hertfordshire, Hertfordshire, United Kingdom*
^{41}*Bhabha Atomic Research Centre (BARC), Mumbai, India*
^{42}*Australian National University, Canberra, Australia*

The ^{72}Ge(n, γ) cross section was measured for neutron energies up to 300 keV at the neutron time-of-flight facility n_TOF (CERN), Geneva, for the first time covering energies relevant to heavy-element synthesis in stars. The measurement was performed at the high-resolution beamline EAR-1, using an isotopically enriched ^{72}GeO$_2$ sample. The prompt capture γ rays were detected with four liquid scintillation detectors, optimized for low neutron sensitivity. We determined resonance capture kernels up to a neutron energy of 43 keV, and averaged cross sections from 43 to 300 keV. Maxwellian-averaged cross section values were calculated from $kT = 5$ to 100 keV, with uncertainties between 3.2% and 7.1%. The new results significantly reduce uncertainties of abundances produced in the slow neutron capture process in massive stars.

I. INTRODUCTION

The chemical elements heavier than Fe are predominantly produced by neutron capture processes in stars and stellar explosions. About half of the abundances are formed in the slow neutron capture process (*s* process) at low neutron densities of 10^7 to 10^{12} cm^{-3} in quiescent burning phases of stars [1–3]. In these environments, neutron capture rates are typically smaller than β-decay rates, which means that the reaction path closely follows the valley of stability on the nuclear chart. The *s* process consists of three components: the main component occurs during H and He shell burning phases in low-mass asymptotic giant branch (AGB) stars, at temperatures of about 0.09 and 0.3 GK, respectively (1 GK = 10^9 K) [4]. This component is responsible for *s* abundances of elements between mass number 90 to 210. The high neutron exposures reached allow the establishment of a reaction flow equilibrium of the form $N \times$ MACS $\approx$ const, where N is the abundance produced in the *s* process, and MACS is the Maxwellian-averaged cross section, i.e., the neutron capture cross section averaged over the stellar neutron velocity distribution. The weak component of the *s* process occurs in massive stars during He core burning at around 0.3 GK temperature and during C shell burning at around 1 GK, and produces elements between mass numbers 60 and 90 [5–8]. Neutron exposures are too small for a reaction flow equilibrium to be established, which means that neutron capture cross sections are key to determine abundances for all isotopes along the reaction path. Finally, the strong component is responsible for the production of Pb and takes place in low metallicity AGB stars [9].

The other half of heavy element abundances is produced by the rapid neutron capture process (*r* process), a sequence of neutron capture reactions at high neutron densities of about 10^{26} cm^{-3} [10]. Nuclear reactions involve mainly radioactive nuclides, thus experimental information on nuclear properties is scarce. The stellar sources of *r* nuclei are still a matter of debate; however, recent observations suggest neutron star mergers as a production site [11,12]. As *r*-process abundances cannot be reliably predicted, they are usually calculated by subtracting calculated *s*-process abundances off the solar abundance pattern [13].

In the last 20 years, there has been significant progress in measuring high precision neutron capture cross sections of intermediate mass nuclei relevant for weak *s*-process nucleosynthesis [1]. However, at present, there are no experimental data on ^{72}Ge(n, γ) covering the entire astrophysical energy range. Experimental data on ^{72}Ge $+n$ reactions include transmission data obtained for natural germanium by Harvey and Hockaday [14], providing total cross sections over a wide energy range from 6 eV to 178 keV. Maletski *et al.* [15] performed transmission and capture measurements on ^{72}Ge and identified 14 resonances up to 30 keV neutron energy, but radiative widths Γ_γ are only known for three resonances up to 4 keV. Consequently, MACS values used in stellar models are exclusively based on theoretical predictions or evaluations taking into account the experimental information available at lower neutron energies. The latest version of the Karlsruhe Astrophysical Database KADoNiS-v1.0 [16] estimates an uncertainty of 25% for their recommended MACS values, which was determined by averaging recent evaluations (TENDL-2015 [17,18], ENDF/B-VII.1 [19], JENDL-4.0 [20]). Individual predicted values for the MACS at $kT = 30$ keV range from 39 mb [21] to 118 mb [22,23].

To reliably calculate abundances of isotopes from germanium to zirconium produced in the weak *s*-process component, accurate stellar neutron capture cross sections on germanium isotopes are indispensable. In addition, recent studies identified the ^{72}Ge(n, γ) reaction as a key reaction determining the uncertainty of ^{72}Ge produced in the *s* process, both in massive stars [24] and in AGB stars [25]. Accurate knowledge of the ^{72}Ge *s* abundance is also critical to determine the ^{72}Ge abundance produced in the *r* process, which has been found to play a decisive role in powering the light curve of the kilonova emission observed following the binary neutron star merger event GW170817 [26]. This paper presents new resonance and cross section data for the ^{72}Ge(n, γ) reaction obtained at the CERN n_TOF facility, continuing on from recently published results on ^{73}Ge(n, γ) [27] and ^{70}Ge(n, γ) [28].

II. EXPERIMENT AT n_TOF

The ^{72}Ge(n, γ) cross section was measured at the neutron time-of-flight facility n_TOF, located at CERN [29]. At n_TOF, neutrons are produced by spallation reactions of a highly energetic (20 GeV), pulsed proton beam from the CERN Proton Synchrotron (PS) impinging on a massive 1.3 ton Pb target. The target is surrounded by 1 cm water and 4 cm borated water layers which serve to cool the target and moderate the neutron flux to achieve a high intensity neutron energy spectrum from 25 meV to several GeV. The measurement was performed at Experimental Area 1 (EAR-1) at a nominal flight path of 185 m, taking advantage of the excellent neutron energy resolution in the energy range of interest (0.11% at 10 keV neutron energy [29]).

The prompt γ rays following a neutron capture event were detected by a set of four liquid scintillation detectors filled with about 1 liter of deuterated benzene (C_6D_6) each. The detectors have been specially optimized for neutron capture measurements to achieve a low sensitivity to background from neutrons scattered into the detector [30,31]. The detectors were installed 7.7 cm upstream from the sample resulting in a position corresponding to an effective angle of 125° relative to the neutron beam.

The capture sample, with a mass of 2.68 g, consisted of 96.59% isotopically enriched ^{72}GeO$_2$ powder, which was pressed into a cylindrical pellet of 2 cm diameter. In addition, data were taken with a metallic Ge sample of natural composition which was used to identify resonances due to other Ge isotopes present in the sample, and an Au sample which was used to normalize the capture yield (both cylindrical with 2 cm diameter). All samples were glued on to a sample holder with 6 μm Mylar backing. To determine the background induced by the sample holder, measurements with an empty sample holder were performed as well.

The neutron flux was continuously monitored using ^{6}Li$(n, t)\alpha$ reactions in a thin 300 μg/cm^2 LiF foil in the beam in conjunction with a set of silicon detectors placed outside the beam. The neutron flux spectrum was measured in a dedicated campaign: in addition to the silicon detection system mentioned above, the flux was also measured with a Micromegas detector using the reference reactions ^{10}B(n, α)

and ^{235}U(n, f) and an ionization chamber by Physikalisch-Technische Bundesanstalt (PTB) Braunschweig measuring ^{235}U(n, f) reactions. The neutron flux spectrum determined by combining all these results has a systematic uncertainty of 2% for neutron energies <10 keV and >100 keV, and of up to 5% between 10 and 100 keV [32]. The methodology of the neutron flux evaluation at n_TOF is described in Ref. [32].

III. DATA ANALYSIS AND RESULTS

The time of flight spectra were converted to neutron energy (E_n) spectra, using the flight path $L = 183.96\,(4)$ m which was determined using well-known low energy resonances in the ^{197}Au(n, γ) reaction [33]. The energy dependent neutron capture yield, defined as the probability for a neutron to undergo radiative capture in the sample, was calculated using

$$\mathbf{Y}(E_n) = f_N(E_n) \frac{\mathbf{C}(E_n) - \mathbf{B}(E_n)}{\varepsilon \Phi_n(E_n)}. \tag{1}$$

Here, $\mathbf{C}$ is the ^{72}Ge sample count rate, $\mathbf{B}$ is the background, ε is the efficiency to detect a capture event, Φ_n is the neutron flux, and $f_N(E_n)$ is a normalization factor.

The efficiency of the capture setup was taken into account using the total energy detection principle [34,35]. For a detection system where (i) the detection efficiency for a single γ ray is proportional to its energy, (ii) the detection efficiency is small, and (iii) at most one γ ray per capture cascade is detected, it can be shown that the efficiency to detect a capture event ε is proportional to the excitation energy of the compound system. While (ii) and (iii) apply to the C_6D_6 system, condition (i) can be achieved by applying weighting factors to the detected signal amplitudes. This approach is called the pulse height weighting technique [35]. Weighting factors were determined by simulating the detector response in GEANT4 [36] for a range of initial γ-ray energies, taking into account the geometry of the experimental setup. Corrections need to be applied for γ-ray signals below the detection threshold (in this case 200 keV) and for transitions without γ-ray emission (electron conversion). Correction factors were determined by simulating capture cascades using the code DICEBOX [37].

The normalization factor f_N accounts for the fact that the neutron beam is larger than the capture sample, and is determined using the saturated resonance technique [38]. The ^{197}Au(n, γ) reaction has a strong resonance at 4.9 eV neutron energy, for which the radiative width Γ_γ is much larger than the neutron width Γ_n. The ^{197}Au(n, γ) capture yield is measured using a sample of sufficient thickness so that all neutrons at the resonance energy react with the sample, providing an absolute measure of the number of neutrons traversing the sample. Since the neutron beam size slightly varies with neutron energy, the normalization factor is energy dependent. These small corrections with respect to the 4.9 eV normalization point (<2% in energy region of interest) were determined in simulations and verified experimentally [29].

The background consists of several components. Background induced by ambient radioactivity and cosmic rays is
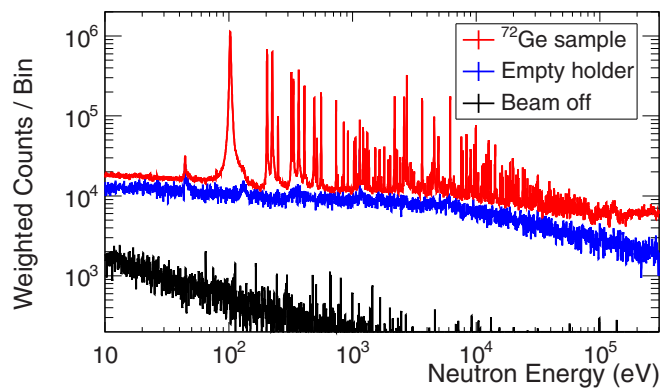
FIG. 1. ^{72}Ge sample spectrum compared to backgrounds due to ambient radioactivity (Beam off) and neutron reactions on the sample holder (Empty holder).

determined in runs without the neutron beam. Background related to the neutron beam is determined in runs with an empty sample holder. The ^{72}Ge count spectrum, compared to both these components, is shown in Fig. 1 (weighting factors have been applied to all spectra).

Another background component comes from neutrons scattered off the ^{72}GeO$_2$ sample which are subsequently captured elsewhere in the experimental area and produce background γ rays. The capture detectors and their support have been optimized to have minimum sensitivity to neutron capture [30,31]; however, neutrons may be captured on other structural material such as the walls of the experimental area. At low neutron energy, where resonances can be resolved with high resolution (resolved resonance region), this background is taken into account by including a constant background to the resonance fit. In the unresolved resonance region where we determined averaged cross sections, the background is estimated using neutron filters. Neutron filters consist of material with strong neutron resonances. They are placed into the neutron beam upstream of the capture sample and are chosen to be thick enough to block out all neutrons at certain resonance energies. Any counts measured in the filter dips consequently come from background of scattered neutrons. The background was determined from the filter dips due to strong resonances in Al around 35, 90, and 160 keV neutron energy and is at the level of 5–15 % compared to the sample spectrum in the region from 43 to 300 keV.

The yield in the resolved resonance region was analyzed with the multilevel, multichannel R-matrix software SAMMY [39]. SAMMY fits resonance shapes taking into account all experimental effects such as resolution broadening, self-shielding, multiple interactions, and sample impurities (e.g., other Ge isotopes). Resonances due to impurities are identified by comparing the capture yield of the enriched ^{72}Ge sample with the spectrum recorded with germanium of natural isotopic composition (background due to oxygen is negligible due to small neutron cross sections). Resonances were fitted using the Reich-Moore approximation and assuming a constant background. Capture data do not usually allow one to reliably determine all individual resonance parameters (gamma and neutron widths, energy, spin, and parity; neutron

TABLE I. Resonance energies E_r and kernels k below 20 keV. The uncertainties listed are from the fitting procedure. In addition, systematic uncertainties of k (not included in the Table) are 3.2% (5.6%) below (above) 10 keV, as described in the text.

E_r (eV)	k (meV)	E_r (eV)	k (meV)
250.290(10)	0.322(7)	10410.1(0.7)	32(3)
738.323(13)	3.62(5)	10959.7(13)	16(3)
1255.76(5)	2.30(7)	11229.9(10)	153(9)
2191.95(2)	40.9(4)	11527.1(4)	66(3)
2428.98(12)	3.6(2)	12064.4(6)	63(5)
2620.85(3)	123.3(14)	12101.8(9)	189(11)
2756.789(14)	185.3(19)	12611.2(2)	268(11)
2810.6(3)	2.6(2)	13160.0(4)	99(5)
2958.38(17)	3.9(2)	14177.3(9)	151(10)
3659.60(5)	131.1(19)	14265.8(3)	278(12)
4404.46(18)	14.4(6)	14602.9(2)	28(23)
4579.4(3)	232(5)	15631.2(8)	74(6)
4963.7(4)	145(4)	15908.0(4)	158(10)
5569.9(8)	5.0(9)	16241.4(8)	172(12)
6176.75(5)	291(6)	16423.9(6)	146(10)
7598.80(12)	102(3)	17401.1(17)	167(15)
7838.67(20)	54(2)	17474.8(13)	35(5)
8258.7(5)	20.0(15)	17938.4(13)	92(7)
8345.80(12)	137(5)	18784.1(5)	218(14)
9022.4(11)	260(11)	19180(6)	184(28)
9645.81(19)	138(6)	19742.7(7)	316(21)
9704.3(3)	169(7)	19978.1(6)	231(15)
9948.46(13)	238(7)		

orbital momentum). Thus we report in Tables I and II only well determined observables for each resonance: resonance energy and capture kernel k, defined as

$$k = g\frac{\Gamma_\gamma \Gamma_n}{\Gamma_\gamma + \Gamma_n}, \quad \text{with } g = \frac{2J + 1}{(2I + 1)(2s + 1)}, \quad (2)$$

with J, I, and s being the resonance, target and neutron spin, respectively.

In total, 93 resonance kernels were determined, with 77 resonances not listed in any database. Figure 2 shows examples of SAMMY fits in the keV neutron energy region. Systematic uncertainties of capture kernels (not included in uncertainties in Tables I and II) are due to the neutron flux (2% below 10 keV and 5% between 10 and 43 keV), the sample enrichment (1%), the normalization (1%), and the pulse height weighting technique (2%) [35], resulting in total systematic uncertainties of 3.2% below and 5.6% above 10 keV neutron energy.

Average resonance parameters were determined using the resonances below 20 keV assuming there are no unresolved doublets. As no spin assignment for resonances is available, during determination of the average radiative width $\overline{\Gamma_\gamma}$ we relied on the assumption that the strongest resonances (in terms of Γ_n) are of s-wave character and on the predictions of statistical model simulations performed using the code DICEBOX [37]. These simulations indicated that $\overline{\Gamma_\gamma^{J^\pi}}$ are very similar for resonances with all J^π and they come from a normal distribution with standard deviation σ_{Γ_γ} which is at most

TABLE II. Resonance energies E_r and kernels k above 20 keV. The uncertainties listed are from the fitting procedure. In addition, systematic uncertainties of k (not included in the Table) are 5.6%, as described in the text.

E_r (eV)	k (meV)	E_r (eV)	k (meV)
20326.5(20)	85(11)	33251(2)	331(39)
21096.7(14)	122(14)	33716(8)	180(45)
21367(3)	69(14)	33843(3)	291(48)
21457.0(12)	97(9)	33974(15)	246(68)
21756.9(15)	240(17)	34163.6(11)	65(24)
21948.4(11)	146(12)	34757(6)	414(65)
23812.5(8)	268(17)	35150(9)	95(33)
24213.6(11)	284(19)	35293(7)	95(31)
24744.5(18)	283(24)	35420(4)	327(46)
25604(3)	149(17)	36465(4)	190(30)
26033(3)	252(21)	36635(6)	168(35)
27026(5)	38(18)	37175(4)	256(45)
27455(3)	189(23)	37495.0(4)	42(18)
28380(3)	102(18)	38206(5)	191(43)
28933(2)	141(16)	39096(4)	434(57)
29492(11)	98(28)	39207(17)	136(59)
29647(4)	147(22)	39311(4)	434(54)
30675(3)	176(25)	39976(4)	320(42)
31037(2)	318(30)	40302(16)	195(53)
31269(3)	118(18)	40960(7)	421(58)
31509(2)	324(30)	41458(5)	112(29)
31651(3)	213(26)	42229(7)	182(34)
32797(3)	170(22)	42577(4)	299(42)
32907(5)	93(17)	42750(4)	442(45)

FIG. 2. Examples of resonance fits of the neutron capture yield using the *R*-matrix code SAMMY [39]. The data are compared to the yield calculated from resonance parameters listed in the ENDF/B-VIII.0 evaluation [33]. The bottom panel shows an example of resonances measured at n_TOF for the first time.

20% of $\overline{\Gamma_\gamma}$. The strongest resonances were selected using the criterion $\Gamma_n \geqslant 10 \times \Gamma_\gamma$, to ensure that the capture kernel k is also a good measure of the radiative width, because for such a criterion $k \approx g\Gamma_\gamma$. The resulting set of radiative widths was fitted using the maximum-likelihood approach (see [40] for details), yielding $\overline{\Gamma_\gamma} = 177(10)$ meV and $\sigma_{\Gamma_\gamma} = 52(8)$ meV. Our value of $\overline{\Gamma_\gamma}$ is $\approx$18% higher than the literature value 150(25) meV [41].

The sum of reduced neutron widths of the above mentioned strongest resonances gives an s-wave neutron strength function $S_0 \approx 1.3(5) \times 10^{-4}$ in agreement with $S_0 \approx 1.39(54) \times 10^{-4}$ available in [42]. The other average resonance parameters were determined similarly to Ref. [43], that is using the statistical model simulations of resonance sequences (assuming the above determined $\overline{\Gamma_\gamma}$, σ_{Γ_γ}, and S_0 values) and comparing the number of observed resonances above a certain threshold in k. Assuming that the kernel for resonances below 20 keV with $J = 1/2$ cannot be higher than 300 meV, i.e., $\Gamma_\gamma \lesssim \overline{\Gamma_\gamma} + 2.5\sigma_{\Gamma_\gamma}$, we observe four strong (with $\Gamma_n \gg \Gamma_\gamma$) p-wave resonances with $J = 3/2$. Their presence imposes a limit of $S_1 \gtrsim 0.7 \times 10^{-4}$, the most probable S_1 value being about two times higher. Using these neutron strength functions we arrived at an s-wave resonance spacing of $D_0 = 1800(300)$ eV. The available literature values of 1190(290) [41] and 2070(290) eV [42] are inconsistent due to the lack of experimental data.
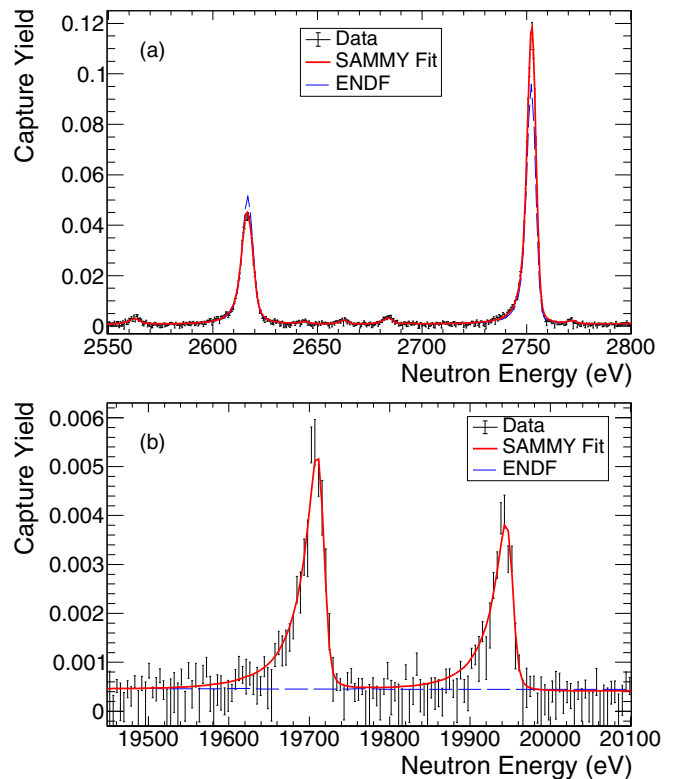
In general, resonances were well separated up to neutron energies of 43 keV. At higher energies, individual resonances cannot be reliably identified, and instead we determined averaged cross sections. Background due to sample impurities (non-negligible contributions come from ^{73}Ge and ^{70}Ge with 2.86% and 0.35% abundance, respectively) was subtracted using recently determined cross sections [27,28]. Multiple interaction and self-shielding corrections were determined in Monte-Carlo simulations, in the same way as described in [27,28]. Figure 3 shows the cross section with statistical uncertainties determined in this work compared to the recent evaluations ENDF/B-VIII.0 [33] and TENDL-2017 [17,44]. Total systematic uncertainties of our averaged cross sections are 6.6–10.4 %. These are due to the neutron filter background (3.9–9.5 %), multiple interaction and self-shielding corrections (1.3%), and sample impurity corrections (1.3%), in addition to the 5.6% or 3.2% systematic uncertainty also applying to the capture kernel (see above). Our data are on average 15–17 % systematically lower than the ENDF ones, e.g., 16% on average from 200 to 300 keV. Likewise, TENDL overestimated the cross section by 27% over the whole URR neutron energy range, on average by about 29% from 50 to 100 keV, and up to 25% from 200 to 300 keV. Tabulated data will be provided to the IAEA EXFOR database [45].
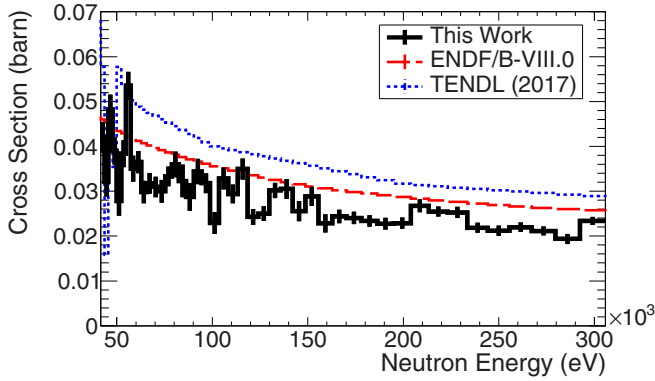
FIG. 3. Averaged cross sections with statistical uncertainties from 43 to 300 keV neutron energy compared to ENDF/B-VIII.0 [33] and TENDL-2017 [17,44]. See text for details.
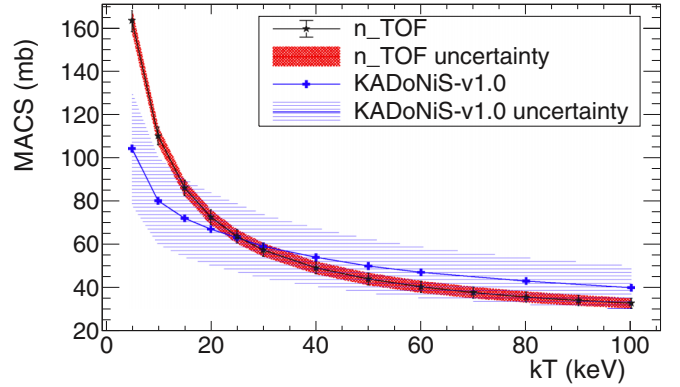

FIG. 4. Maxwellian-averaged cross sections of this work (n_TOF) from $kT = 5$ to 100 keV compared to MACS values recommended in the latest version of the database KADoNiS-v1.0 [16].

IV. MAXWELLIAN-AVERAGED CROSS SECTION AND ASTROPHYSICAL IMPLICATIONS

We calculated Maxwellian-averaged cross sections using

$$\text{MACS} = \frac{2}{\sqrt{\pi}} \frac{1}{(kT)^2} \int_0^\infty \sigma(E_n) E_n \exp\left(-\frac{E_n}{kT}\right) dE_n \quad (3)$$

for kT values up to 100 keV. The cross section contribution from outside the experimental range (>300 keV) was taken from the ENDF/B-VIII.0 [33] evaluation, but scaled by 0.84 to match the experimentally determined cross section at lower energies. The contribution of the scaled ENDF cross section to the MACS is negligible up to $kT \leqslant 50$ keV and between 2.5% and 14.7% from 60 to 100 keV. MACS values, and total (systematic and statistical) uncertainties, are listed in Table III and shown in Fig. 4, with a 20% uncertainty assumed for the scaled ENDF cross section data. Our results are compared to MACS values recommended in KADoNiS-v1.0 [16], which exhibit a flatter energy dependence as a function of kT. The largest discrepancies of up to 60% are in the lower energy

TABLE III. Maxwellian-averaged cross sections and total uncertainties (systematic and statistical) from $kT = 5$ to 100 keV compared to MACSs recommended in KADoNiS-v1.0 [16].

	MACS (mb)	
kT (keV)	This work	KADoNiS-v1.0 [16]
5	162.9 ± 5.1	104 ± 26
10	109.9 ± 4.1	80 ± 20
15	86.0 ± 3.6	72 ± 18
20	72.4 ± 3.4	67 ± 17
25	63.6 ± 3.2	63 ± 16
30	57.4 ± 3.0	59 ± 15
40	49.2 ± 2.9	54 ± 14
50	44.0 ± 2.8	50 ± 13
60	40.4 ± 2.7	47 ± 12
70	37.7 ± 2.6	
80	35.7 ± 2.5	43 ± 11
90	34.1 ± 2.4	
100	32.9 ± 2.3	40 ± 10

region ($\leqslant 20$ keV), while at higher kT values agreement is within 10–20%. The n_TOF energy trend is more similar to the older evaluation of KADoNiS-v0.3 based on Ref. [46], but about 20% smaller overall. However, the new result of 57.4 ± 3.0 mb at $kT = 30$ keV is within 3% agreement with the KADoNiS-v1.0 estimation.

The impact of our new cross section data on stellar abundances has been investigated using a 25 solar mass star with 2% metallicity, modeled with the code MESA [47]. The weak *s*-process nucleosynthesis was calculated with the post-processing code MPPNP [48]. We have calculated abundances produced in the *s* process using the ^{72}Ge(n, γ) MACS values recommended by KADoNiS-v1.0 and with the new MACSs determined in this work. We show the impact on both burning stages where the *s* process takes place: *s*-process nucleosynthesis occurs first towards the end of He core burning ($\approx 7 \times 10^5$ years duration) via ^{22}Ne(α, n) reactions with neutron densities of $\approx 10^7$ cm^{-3} and temperatures of 0.3 GK ($kT \approx 26$ keV). The material is later reprocessed during C shell burning at around 1 GK ($kT \approx 90$ keV), where the ^{22}Ne(α, n) neutron source is reactivated. During this shorter *s*-process phase (≈ 600 years) neutron densities reach 10^{11} to 10^{12} cm^{-3} [3,6,49]. Figure 5(a) shows abundances of *s*-process isotopes between mass 70 and 96 after He core burning, using ^{72}Ge(n, γ) MACSs of this work, relative to abundances obtained using KADoNiS-v1.0. Coincidentally, the new MACS value at 25 keV is in very good agreement with KADoNiS-v1.0, therefore we only observe abundance changes of 1–2 % after He-core burning. The results include error bands indicating the abundance uncertainty due to uncertainties in the ^{72}Ge(n, γ) MACS, which are 25% for KADoNiS-v1.0 and 5% for results of this work. The figure clearly demonstrates that abundance uncertainties due to the cross section are now significantly reduced.

Figure 5(b) shows abundance ratios after C shell burning, during which *s*-process material produced during He core burning is reprocessed at higher temperatures of about $kT = 90$ keV. The smaller MACS of this work compared to KADoNiS-v1.0 leads to final ^{72}Ge abundances that are 14% higher, while heavier isotope abundances along the reaction path are affected by up to 7%. This panel does not include
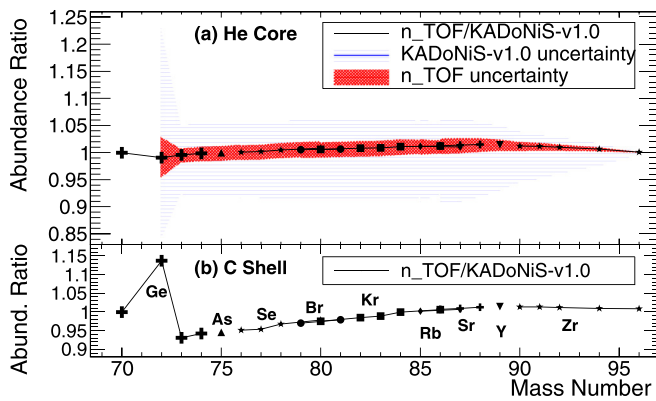
FIG. 5. Abundances produced in the *s* process for a 25 solar mass star using the new cross sections determined at n_TOF. Abundances are normalized to results using the ^{72}Ge(n, γ) MACSs recommended in KADoNiS-v1.0 [16]. Isotopes of the same elements are connected by thin solid lines. Panel (a) shows abundances after He core burning. The shaded areas represent abundance variations when taking into account uncertainties of KADoNiS (blue) or n_TOF (red) cross sections. Panel (b) shows abundances after the later C shell burning phase.

any uncertainty estimation, as final abundances not only depend on MACS values at $kT = 90$ keV but also on the seed abundances that have been produced during the earlier He core burning stage.

In conclusion, we have measured the ^{72}Ge(n, γ) cross section with high precision at the CERN n_TOF facility, and for the first time covered the entire neutron energy range relevant for *s*-process nucleosynthesis. Our results significantly reduce uncertainties in calculations of abundances produced in the weak *s*-process component occurring in quiescent burning phases in massive stars.

[1] R. Reifarth, C. Lederer, and F. Käppeler, Neutron reactions in astrophysics, J. Phys. G **41**, 053101 (2014).

[2] F. Käppeler, R. Gallino, S. Bisterzo, and W. Aoki, The *s* process: Nuclear physics, stellar models, and observations, Rev. Mod. Phys. **83**, 157 (2011).

[3] M. Pignatari, R. Gallino, M. Heil, M. Wiescher, F. Käppeler, F. Herwig, and S. Bisterzo, The weak s-process in massive stars and its dependence on the neutron capture cross sections, Astrophys. J. **710**, 1557 (2010).

[4] F. Herwig, Evolution of asymptotic giant branch stars, Annu. Rev. Astron. Astrophys. **43**, 435 (2005).

[5] C. M. Raiteri, M. Busso, R. Gallino, G. Picchio, and L. Pulone, S-process nucleosynthesis in massive stars and the weak component. I. Evolution and neutron captures in a 25 M$_{sun}$ star, Astrophys. J. **367**, 228 (1991).

[6] C. M. Raiteri, M. Busso, R. Gallino, and G. Picchio, S-process nucleosynthesis in massive stars and the weak component. II. Carbon burning and galactic enrichment, Astrophys. J. **371**, 665 (1991).

[7] C. M. Raiteri, R. Gallino, and M. Busso, S-processing in massive stars as a function of metallicity and interpretation of observational trends, Astrophys. J. **387**, 263 (1992).

[8] C. M. Raiteri, R. Gallino, M. Busso, D. Neuberger, and F. Käppeler, The weak s-component and nucleosynthesis in massive stars, Astrophys. J. **419**, 207 (1993).

[9] C. Travaglio, R. Gallino, M. Busso, and R. Gratton, Lead: Asymptotic giant branch production and galactic chemical evolution, Astrophys. J. **549**, 346 (2001).

[10] J. J. Cowan, C. Sneden, J. E. Lawler, A. Aprahamian, M. Wiescher, K. Langanke, G. Martínez-Pinedo, and F.-K. Thielemann, Origin of the heaviest elements: The rapid neutron-capture process, Rev. Mod. Phys. **93**, 015002 (2021).

[11] E. Pian *et al.*, Spectroscopic identification of r-process nucleosynthesis in a double neutron-star merger, Nature (London) **551**, 67 (2017).

[12] D. Watson, C. Hansen, J. Selsing *et al.*, Identification of strontium in the merger of two neutron stars, Nature (London) **574**, 497 (2019).

[13] N. Prantzos, C. Abia, S. Cristallo, M. Limongi, and A. Chieffi, Chemical evolution with rotating massive star yields II. A new assessment of the solar s- and r-process components, Mon. Not. R. Astron. Soc. **491**, 1832 (2020).

[14] J. Harvey and M. Hockaday, 1980, EXFOR entry 13770.004.

[15] K. Maletski, L. B. Pikelner, I. M. Salamatin, and E. I. Sharapov, Neutron cross sections and strength functions for germanium isotopes, Sov. J. At. Energy **24**, 207 (1968).

[16] I. Dillmann *et al.*, The Karlsruhe astrophysical database of nucleosynthesis in stars project - status and prospects, Nucl. Data Sheets **120**, 171 (2014).

[17] A. J. Koning and D. Rochman, Modern nuclear data evaluation with the TALYS code system, Nucl. Data Sheets **113**, 2841 (2012).

[18] A. J. Koning *et al.*, TENDL-2015: TALYS-based evaluated nuclear data library (2016), https://tendl.web.psi.ch/tendl_2015/tendl2015.html.

[19] M. B. Chadwick *et al.*, ENDF/B-VII.1 nuclear data for science and technology: Cross sections, covariances, fission product yields and decay data, Nucl. Data Sheets **112**, 2887 (2011).

[20] K. Shibata *et al.*, JENDL-4.0: A new library for nuclear science and engineering, J. Nucl. Sci. Technol. **48**, 1 (2011).

[21] S. E. Woosley, W. A. Fowler, J. A. Holmes, and B. A. Zimmerman, Semiempirical thermonuclear reaction-rate data for intermediate-mass nuclei, At. Data Nucl. Data Tables **22**, 371 (1978).

[22] S. Goriely, Improved predictions of neutron capture rates and their impact on the s- and r-process nucleosynthesis, PoS (**NIC V**), 314 (1998).

[23] M. Aikawa, M. Arnould, S. Goriely, A. Jorissen, and K. Takahashi, BRUSLIB and NETGEN: The Brussels nuclear reaction rate library and nuclear network generator for astrophysics, Astron. Astrophys. **441**, 1195 (2005).

[24] N. Nishimura *et al.*, Uncertainties in s-process nucleosynthesis in massive stars determined by Monte Carlo variations, Mon. Not. R. Astron. Soc **469**, 1752 (2017).

[25] G. Cescutti *et al.*, Uncertainties in s-process nucleosynthesis in low-mass stars determined from Monte Carlo variations, Mon. Not. R. Astron. Soc **478**, 4101 (2018).

[26] M. R. Wu, J. Barnes, G. Martínez-Pinedo, and B. D. Metzger, Fingerprints of Heavy-Element Nucleosynthesis in the Late-Time Lightcurves of Kilonovae, Phys. Rev. Lett. **122**, 062701 (2019).

[27] C. Lederer-Woods *et al.* (n_TOF Collaboration), Measurement of ^{73}Ge(n, γ) cross sections and implications for stellar nucleosynthesis, Phys. Lett. B **790**, 458 (2019).

[28] A. Gawlik *et al.* (n_TOF Collaboration), Measurement of the ^{70}Ge(n, γ) cross section up to 300 keV at the CERn n_TOF facility, Phys. Rev. C **100**, 045804 (2019).

[29] C. Guerrero *et al.* (n_TOF Collaboration), Performance of the neutron time-of-flight facility n_TOF at CERN, Eur. Phys. J. A **49**, 27 (2013).

[30] R. Plag, M. Heil, F. Käppeler, P. Pavlopoulos, R. Reifarth, and K. Wisshak, An optimized C_6D_6 detector for studies of resonance-dominated (n, γ) cross-sections, Nucl. Instrum. Methods Phys. Res. A **496**, 425 (2003).

[31] P. F. Mastinu *et al.*, New C_6D_6 Detectors: Reduced Neutron Sensitivity and Improved Safety, CERN Report No. CERN-n_TOF-PUB-2013-002 (CERN, Geneva, 2013).

[32] M. Barbagallo *et al.* (n_TOF Collaboration), High-accuracy determination of the neutron flux at n_TOF, Eur. Phys. J. A **49**, 156 (2013).

[33] D. Brown *et al.*, ENDF/B-VIII.0: The 8th major release of the nuclear reaction data library with CIELO-project cross sections, new standards and thermal scattering data, Nucl. Data Sheets **148**, 1 (2018).

[34] R. L. Macklin and J. H. Gibbons, Capture-cross-section studies for 30–220 keV neutrons using a new technique, Phys. Rev. **159**, 1007 (1967).

[35] U. Abbondanno *et al.* (n_TOF Collaboration), New experimental validation of the pulse height weighting technique for capture cross-section measurements, Nucl. Instrum. Methods Phys. Res. A **521**, 454 (2004).

[36] S. Agostinelli *et al.* (Geant4 Collaboration), GEANT4 – a simulation toolkit, Nucl. Instrum. Methods Phys. Res. A **506**, 250 (2003).

[37] F. Bečvář, Simulation of γ cascades in complex nuclei with emphasis on assessment of uncertainties of cascade-related quantities, Nucl. Instrum. Methods A **417**, 434 (1998).

[38] R. L. Macklin *et al.*, Absolute neutron capture yield calibration, Nucl. Instrum. Methods A **164**, 213 (1979).

[39] N. Larson, Updated Users Guide for SAMMY: Multilevel R-Matrix Fits to Neutron Data Using Bayes Equations, Technical Report ORNL/TM-9179/R8 (Oak Ridge National Laboratory, Oak Ridge, TN, 2008).

[40] M. Mastromarco *et al.* (n_TOF Collaboration), Cross section measurements of ^{155,157}Gd(n, γ) induced by thermal and epithermal neutrons, Eur. Phys. J. A **55**, 9 (2019).

[41] S. Mughabghab, *Atlas of Neutron Resonances*, 6th ed., Vol. 1 (Elsevier, Amsterdam, 2018).

[42] S. Mughabghab, *Atlas of Neutron Resonances*, 5th ed. (Elsevier, Amsterdam, 2006).

[43] J. Lerendegui-Marco *et al.* (n_TOF Collaboration), Radiative neutron capture on ^{242}Pu in the resonance region at the CERN n_TOF-EAR1 facility, Phys. Rev. C **97**, 024605 (2018).

[44] D. Rochman *et al.*, The TENDL library: Hope, reality and future, EPJ Web Conf. **146**, 02006 (2017).

[45] N. Otuka *et al.*, Towards a more complete and accurate experimental nuclear reaction data library (EXFOR): International collaboration between nuclear reaction data centres (NRDC), Nucl. Data Sheets **120**, 272 (2014).

[46] Z. Bao *et al.*, Neutron cross sections for nucleosynthesis studies, At. Data Nucl. Data Tables **76**, 70 (2000).

[47] C. Ritter, F. Herwig, R. Hirschi, S. Jones, C. Fryer, and M. Pignatari, NuGrid stellar data set – II. Stellar yields from H to Bi for stellar models with $M_{ZAMS} = 1-25\,M_\odot$ and $Z = 0.0001-0.02$, Mon. Not. R. Astron. Soc **480**, 538 (2018).

[48] M. Pignatari *et al.*, NuGrid stellar data set. I. Stellar yields from H to Bi for stars with metallicities $Z = 0.02$ and $Z = 0.01$, Astrophys. J., Suppl. Ser. **225**, 24 (2016).

[49] N. Prantzos, M. Hashimoto, and K. Nomoto, The s-process in massive stars: Yields as a function of stellar mass and metallicity, Astron. Astrophys. **234**, 211 (1990).